

Molecular basis of the chemiluminescence mechanism of luminol

Angelo Giussani,^{*[a]} Pooria Farahani,^[b] Daniel Martínez-Muñoz,^[c] Marcus Lundberg,^[c] Roland Lindh^[c] and Daniel Roca-Sanjuán^{*[a]}

Abstract: Light emission of luminol is probably one of the most popular chemiluminescence reactions due to its use in forensic science, recently displaying promising applications on the treatment of cancer in deep tissues. The mechanism is however very complex and distinct possibilities have been proposed. By efficiently combining DFT and CASPT2 methodologies, we have studied the chemiluminescence mechanism in three steps, (i) luminol oxygenation to generate the chemiluminophore, (ii) chemiexcitation step, and (iii) generation of the light emitter. The findings demonstrate that luminol double deprotonated dianion activates molecular oxygen, that diazaquinone is not formed, and that the chemiluminophore is formed via concerted addition of oxygen and concerted elimination of nitrogen. The peroxide bond in comparison to other isoelectronic chemical functionalities (-NH-NH-, -N-N-, and -S-S-) is found to have the best chemiexcitation efficiency, which allow to rationalize the oxygenation requirement and establishes general design principles for the chemiluminescence efficiency. Electron transfer from the aniline ring to the the OO bond promotes the excitation process creating an excited state which is not the chemiluminescence species. To produce the light emitter, a proton transfer between the amino and carbonyl groups must occur, which is shown to require high localized vibrational energy during the chemiexcitation.

Introduction

Chemiluminescence is the phenomenon of light emission originated from a chemical reaction.^[1] One of the most important and popular chemiluminescent systems is the luminol molecule (5-amino-2,3-dihydrophthalazine-1,4-dione), which is widely used in forensic science to detect traces of blood since it is catalyzed by the iron of the hemoglobin protein.^[1,2] First

discovered in 1928 by Albrecht,^[3] luminol chemiluminescence has been since then the research topic of many fundamental studies, developments of commercial analytical assay kits,^[4-9] and challenging therapeutic procedures to treat cancers in deep tissues.^[10-14] It is worth mentioning in this last context, for example, the investment of hospitals and research groups on finding non-invasively treatment of inaccessible tumors like, for example, the Glioblastoma Multiforme brain tumor, by means of mitochondria-targeting luminol systems.^[10] To assist in such developments, it is crucial a detailed comprehension of the chemiluminescence mechanism and key electronic-structure factors in the chemiexcitation phenomenon. Identifying the factors which favors the excited-state population rather than thermal decomposition shall help to increase the chemiluminescence yield and those that decrease the activation barriers and produce rapid chemiexcitation shall contribute to design ultrasensitive chemiluminescence assays.

Light emission in luminol is observed in solutions in the presence of molecular oxygen under alkaline conditions with or without the presence of an additional co-oxidant, as iron, depending if the molecule is in a protic or aprotic solvent, respectively.^[15-17] In both cases, the reaction produces molecular nitrogen and excited 3-aminophthalate dianion (**3AP**²⁻), whose radiative deactivation from its singlet excited manifold is responsible for the luminol chemiluminescent emission (see Scheme 1a). The role of **3AP**²⁻ as light emitter has been proven by the match between the luminol chemiluminescent spectrum and the fluorescence spectrum of **3AP**²⁻.^[18-20] Despite being originated from the same molecule, a slight difference in the emission spectra is observed when operating in either aprotic or protic solvents.^[18] A blue-shift of the maximum chemiluminescence wavelength is observed in protic environments with respect to aprotic solutions, from 485^[18]/502^[19,20]/510^[21] nm in DMSO to 424^[6,18,21]/431^[19,20] nm in water. Such a difference has been postulated experimentally to be related to an intramolecular hydrogen transfer from the amino group to the nearby oxygen atom that can occur in aprotic solvents.^[18] In general, luminol chemiluminescence is not a process with high probability, being its quantum yield of the order of 10⁻².^[22,23] Nevertheless, as compared to other chemiluminescence systems based on the 1,2-dioxetane and dioxetanone, luminol is considered an efficient chemiluminescent compound.^[22] In this context, knowledge of key chemical groups for an efficient chemiexcitation and the excited-state reaction path that leads to the emitter, together with the non-radiative deactivation processes competing with the emission, undoubtedly constitutes the basis for operating selective chemical modifications aimed at improving the emission quantum yield.

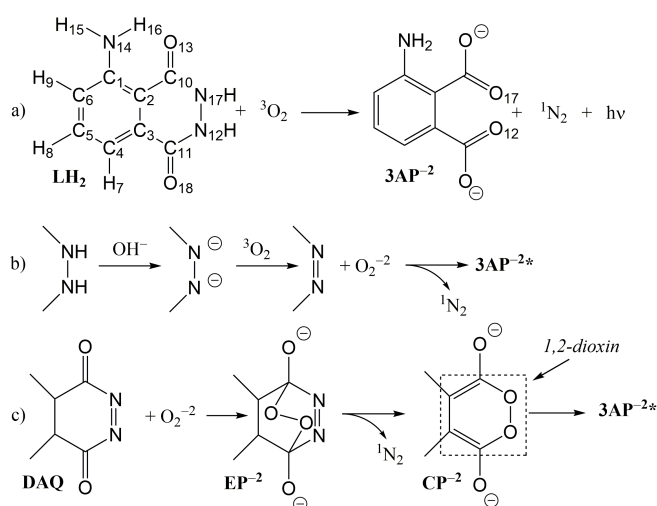
[a] Dr. A. Giussani, Dr. D. Roca-Sanjuán
Institut de Ciència Molecular
Universitat de València

P. O. Box 22085 València, Spain
E-mail: angelo.giussani@uv.es, daniel.roca@uv.es

[b] Dr. Pooria Farahani
Department of Theoretical Chemistry & Biology, School of
Engineering sciences in Chemistry, Biotechnology and Health
(CBH)

KTH Royal Institute of Technology
SE-10691 Stockholm, Sweden

[c] Daniel Martínez-Muñoz, Dr. Marcus Lundberg, Prof. Dr. Roland
Lindh
Department of Chemistry-Ångström Laboratory
Uppsala University
P. O. Box 538, SE-751 21 Uppsala, Sweden



Scheme 1. (a) Luminol chemiluminescent reaction with the atoms numbering used in this work, (b) conventional mechanism involving the generation of peroxide, and (c) reaction step producing the postulated intermediates EP⁻² and the chemiluminophore CP⁻².

The global chemiluminescent process operating in luminol (LH₂) in aprotic media implies the reaction with oxygen (³O₂) leading to the formation of 3AP⁻² in its singlet excited state manifold which subsequently decay by means of a radiative process. According to the currently established (conventional) mechanism in DMSO (see Ref. [15] and reference therein), the first step involves the initial formation of the dianion (L⁻²) and the oxidation by ³O₂ to diazaquinone (DAQ), which further react with the formed peroxide dianion O₂⁻² by means of a nucleophilic addition leading to the excited 3AP⁻² molecule and ¹N₂ elimination, see Scheme 1b^[7,24–26]. The mechanism of chemical excitation is still a matter of debate. The most accepted proposal involves firstly the formation of a bicyclic endoperoxide intermediate (EP⁻²) leading to the formation of the 1,2-dioxane-3,6-dione cyclic peroxide (CP⁻²), and then the population through a thermally activated OO bond breaking of the 3AP⁻² excited states (see Scheme 1c).^[27–30] Despite such a proposal, the mechanism through which the oxygen molecule is supposed to be added into the luminol structure to form CP⁻² has not been clearly elucidated, neither it has not been studied the inherent spin inversion process which activates ³O₂. Furthermore, the chemiexcitation efficiency of the cyclic peroxide bond as compared to that of other isoelectronic chemical functionalities has not been described in detail, which might help to better understand the requirement of forming a peroxide compound rather than other possibilities.

Regarding the chemiexcitation process of CP⁻² and how specifically the OO bond breaking causes the population of the 3AP⁻² excited states, this has only been recently addressed in part by Griesbeck *et al.*^[31] In that study, based on density functional theory (DFT) and the complete-active-space second-order perturbation theory //complete-active-space self-

consistent-field (CASPT2//CASSCF) protocol (CASPT2 energies at CASSCF optimized geometries), the authors found that from the CP⁻² equilibrium structure, the system can easily reach a nearby transition state (TS) related to the peroxide bond stretching. From such TS, the system can next evolve along a plausible path toward a conical intersection (CI) with the low-lying singlet excited state (S₁). The work consequently provides a hint on the chemiexcitation step. Further information is however needed regarding the nature of the involved electronic states which is crucial to clearly establish the chemiexcitation mechanism. In addition, the reported vertical emission energy of the S₁ equilibrium structure, equal to 1.57 eV (corresponding to a 790 nm wavelength), do not agree with the much shorter maximum chemiluminescence wavelengths experimentally recorded (~500^[18–21] nm in DMSO and ~425^[6,18–21] in water).

In the present contribution, the reaction between luminol and molecular oxygen to form CP⁻², the mechanism leading from CP⁻² to the excited 3AP⁻², and its subsequent non-radiative and radiative (chemiluminescence) excited state relaxation routes have been studied by efficiently combining the DFT, CASSCF, and CASPT2 methods with the CASPT2//DFT, CASPT2//CASSCF, and CASPT2//CASPT2 protocols. The focus of the work is to revise the experimentally postulated generation mechanism of the CP⁻² high-energy intermediate, to determine the electronic-structure details of the chemiexcitation process, and to characterize the evolution towards the light emitter. The intrinsic chemiluminescent properties of luminol are pursued here which can be ascribed mainly to the process taking place in aprotic media. Explicit role of hydrogen bonding with solvent molecules is a more complex process which requires first the detailed understanding of the phenomenon in the molecule itself. Nevertheless, some hints shall be also provided for the mechanism in water solution. Furthermore, in this work, the possibility of either a concerted or a stepwise addition of ³O₂ to L⁻² has been explored determining the factors which overcome the spin-forbidden process. The chemiexcitation mechanism leading from the CP⁻² molecule to the population of the 3AP⁻² singlet excited states has been characterized beyond the CASPT2//CASSCF protocol, particularly, including explorations at the fully-correlated CASPT2//CASPT2 level. A complex chemiexcitation region has been determined with two types of CIs (in contrast to the previous finding by Griesbeck *et al.*)^[31] which are key to activate the chemiluminescence. Once the excited state is populated, both a non-radiative decay path and a relaxation towards the light emitter species have been identified. The latter displays a vertical emission energy in agreement with the experimental maximum chemiluminescence wavelengths recorded in DMSO and is characterized by a hydrogen transfer from the amino group to the nearby oxygen atom, consequently validating early proposals in DMSO.^[18]

Results and Discussion

The results obtained in this work and the corresponding discussion shall be organized in four sections. Firstly, the

transformation from $\text{LH}_2/\text{L}^{-2}$ to the chemiluminophore CP^{-2} , is analyzed (*oxygenation step*). Secondly, the efficiency of the

WILEY-VCH

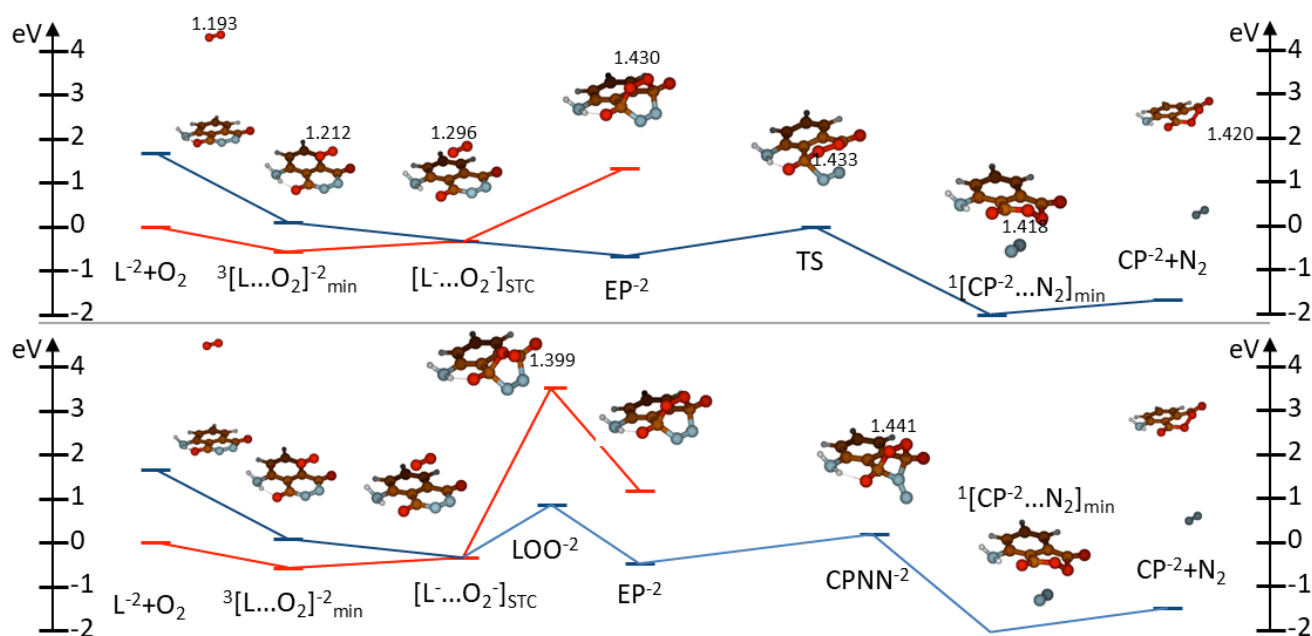


Figure 1. LC-BLYP/6-31G* energy profiles for the triplet and singlet manifolds (red and blue, respectively) supported by CAM-B3LYP and CASPT2 computations and PCM calculations with the DMSO solvent (see Fig. S9) for the $L^{-2} + {}^3O_2 \rightarrow CP^{-2} + {}^1N_2$ reaction process following concerted (top) and step-wise (bottom) mechanisms. Relevant OO bond lengths (in Å) are shown.

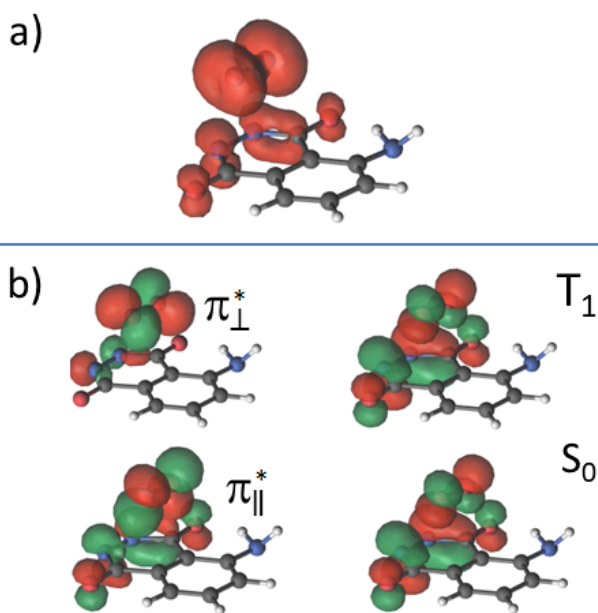


Figure 2. (a) Spin-density representation at the ${}^3[L \dots O_2]^{-2}_{min}$ structure and (b) the two singly-occupied natural orbitals in the triplet and singlet electronic states at the $[L \dots O_2]_{STC}$ crossing obtained with the CASSCF method.

chemiexcitation of the OO peroxide bond is compared with other isoelectronic chemical functionalities containing nitrogen and sulfur atoms. Thirdly, the chemiexcitation mechanism of CP^{-2} is discussed. These two subsections (second and third) corresponds to the *chemiexcitation step*. Finally, the results for the light emission step are presented (*light-emitter generation step*).

Activation of luminol by oxygenation

DFT and CASPT2 computations were carried out to determine the mechanism of the reaction between luminol and 3O_2 to produce the postulated chemilumiphore or high-energy intermediate, CP^{-2} , and 1N_2 . Fig. 1 displays the energy profiles of the lowest-lying singlet (S_1) and triplet (T_1) electronic states along the reaction process and relatives to the separated L^{-2} and 3O_2 as starting reactants. Both step-wise and concerted paths for the attachment of oxygen and elimination of nitrogen are compared. In aprotic media, chemiluminescence of luminol requires strong alkaline conditions to generate L^{-2} ($pK_{a1}=6.7$ and $pK_{a2}=15.1$).^[15] The purpose for that deprotonation is to decrease the ionization potential of LH_2 and allow the reduction of molecular oxygen to activate it. Upon allowing the interaction between the two reactants, a triplet complex, ${}^3[L \dots O_2]^{-2}_{min}$, is formed which has a charge transfer character; from the CASSCF computations, a Mulliken charge of -0.4 is obtained for the 3O_2 moiety. According to the spin densities generated with the CASSCF wave function, the triplet becomes delocalized also over L^{-2} at the reaction complex structure (see Fig. 2a). Such partial electron transfer gives rise to a slight increase of 0.02 Å for the OO bond length. The triplet exciplex formation as the

result of the spin delocalization overcomes the Coulomb repulsion between the charged fragments. Further elongation brings the system to a singlet-triplet crossing (STC) region, $[L^- \dots O_2]_{STC}$, which is easily accessible considering the small energy barrier from the triplet complex. Such STC was obtained as the energy minimum in the singlet manifold using an open-shell approach.^[32,33] At $[L^- \dots O_2]_{STC}$, one electron is completely transferred to the molecular oxygen. According to the analysis of the natural orbitals obtained from the CASSCF computations, the triplet state of $[L^- \dots O_2]_{STC}$ has an unpaired electron in a π orbital of the luminol part and the other at the π^* orbital of the O_2 moiety with a relative perpendicular orientation (π^*_{\perp}), see Fig. 2b. Meanwhile, the singlet state has the unpaired electrons one also in the π orbital of luminol and the other is now in the parallel π^* orbital of oxygen (π^*_{\parallel}). Such orthogonality between π^*_{\perp} and π^*_{\parallel} is optimal according to El-Sayed's rules^[34] for an efficient triplet to singlet transition and it is crucial for the mechanism of oxygenation since it permits the population transfer from the triplet to the singlet manifold and the further reactivity to generate CP^{-2} . CASPT2 computations of the spin-orbit coupling (SOC) at this structure produces a large value of 42 cm^{-1} , which confirms the high probability for the process of spin change. Previous studies [15] indicate the neutral DAQ as an important intermediate for the chemiluminescence mechanism. Different mechanism has been proposed in order to rationalize the DAQ formation [Dani, ref 7-12]; one of the most accredited considers that DAQ is generated together with O_2^{-2} from a double electron transfer from L^{-2} to 3O_2 . Next the formed O_2^{-2} species further attach to the DAQ molecule. However, it is not clear how the spin-forbidden process is overcome in such manner and how the oxygen is activated. The results obtained in this work points to a single electron transfer and L^- and superoxide (O_2^-) as key intermediates, in agreement with the most accepted mechanism proposed for the luminol reaction in DMSO (ref. 15). Such oxygenation mechanism allows to rationalize the spin inversion in previous works on the single electron transfer oxygenation step in the bioluminescence reaction of luciferin in Fireflies^[35] and *Cypridina* luciferin analogues.^[36,37] Moreover, it can be also related to analogous phenomena taking place in other biological processes involving, for example, enzymes with flavin molecules as activators of molecular oxygen.^[38]

Upon reaching ${}^3[L^- \dots O_2]_{STC}$, distinct routes are in principle available for the attachment of the oxygen moiety. The system might either continue the triplet manifold without spin inversion or hop to the singlet potential energy hypersurface (PEH) and continue there. On the other hand, addition of the O_2^- might take place by either a stepwise or concerted mechanism. Addition of O_2^{-2} to DAQ has been proposed to occur in water via the formation of a single bond at the carbonyl group opposite to the amino group site.^[15] Dani, ref 13 However, this aspect of the mechanism must also be modified in the conventional scheme, at least in aprotic media. Such species has not been found in the present computations as a well-defined minimum and formation of the single bond at the other carbonyl (LOO^{-2} , see Figure 1) implies a much higher energy process as compared to the evolution on the singlet surface by a concerted manner which is the most favorable route (see Fig. 1). Further reactivity on the

triplet surface is also not possible. Hence, oxygenation is predicted in this work to take place in a concerted mechanism. Furthermore, the present study supports an asynchronous addition of oxygen and elimination of nitrogen. Regarding the EP^{-2} species (see Figure 1), postulated in the literature as a possible intermediate,^[15] it is found here to be a well-defined equilibrium structure, which can consequently be in principle detected experimentally. From this structure, removal of 1N_2 takes also place by means of a concerted mechanism involving a TS accessible from the initial reactants.

It is also worth analyzing the possibility of a monoanion (or single deprotonated luminol, LH^-) as starting reactant, with the negative charge in N12 (see Scheme 1) since this group has lower pKa. This analysis might be of interest in protic media since L^{-2} is not present in significant quantities due to the strong alkaline conditions required. Nevertheless, some comments are also of interest in aprotic media. Initial structures were also computed by means of the DFT method. Energetics for such species are displayed in Figs. S10-11. As can be seen, the STC crossing is located now at much higher energies as compared to the findings obtained for L^{-2} . This is because LH^- is not as good reduction agent as L^{-2} . The reaction process was also roughly explored in the other monoanion (with the negative charge in N17) finding also a less favorable oxygen addition (Figs. S10-11).

Overall, the concerted oxygenation and 1N_2 elimination taking place from L^{-2} and producing the chemiluminophore CP^{-2} is an exothermic process, with no significant energy barriers, and involves an electron transfer process to overcome the change of spin in the reaction ${}^3O_2 + L^{-2} \rightarrow 3AP^{-2} + {}^1N_2 + h\nu$.

Chemiluminophore efficiency of CP^{-2}

As indicated in the Introduction, a relevant aspect to comprehend the chemiluminescence mechanism of luminol is to explain why the compound needs to be oxidized to produce chemiluminescence and to rationalize the chemiexcitation properties of CP^{-2} . For such purpose, we have isolated the smallest chemical functionality of CP^{-2} which still maintains the chemiexcitation ability. It corresponds to the 1,2-dioxin molecule (see Scheme 1c). This peroxide compound is isoelectronic with molecules containing other atoms such as the protonated and deprotonated diazide, closely related to the parent luminol molecule, and 1,2-dithiin. We shall refer to such small models as -X-X-, where X denotes O, S, NH, or N. Their properties as chemiluminophores shall be analyzed in this section.

By using approximated Walsh diagrams and in line with the general molecular-orbital model of chemiluminescence according to Ref. [1], it is possible to roughly estimate the intrinsic chemiexcitation potential of the mentioned four small models. According to the CASPT2/CASSCF computations,[†] the reactant is not planar and has the X atoms one above the plane of the defined by the carbon atoms and the other below. Ring decomposition takes place by the symmetric bending of the C10C2C3 and C11C3C2 bonds and twisting of the C10C2C3C11 dihedral angle. This means that the symmetry operation preserved along the ring opening is an in-plane C_2 axis perpendicular to the -X-X- bond. Walsh diagrams are thus

drawn considering such symmetry (see Fig. 3). Simplified analyses for an in-plane XX bond breaking can be found in Fig.

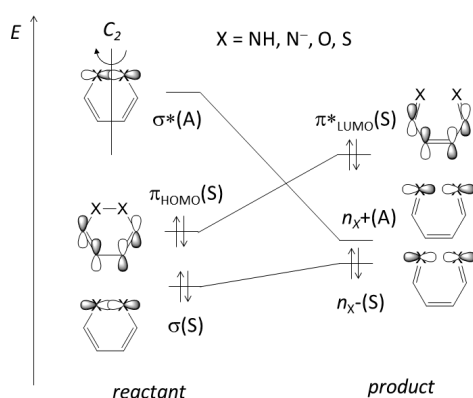


Figure 3. Walsh orbital correlation diagram for the ring opening of 1,2-dioxin and the related small models. The notation (X) denotes for a given orbital the symmetry property X with respect to the C_2 axis which can be either symmetric (S) or antisymmetric (A). A related diagram based on CASSCF natural orbitals is shown in Fig. S14.

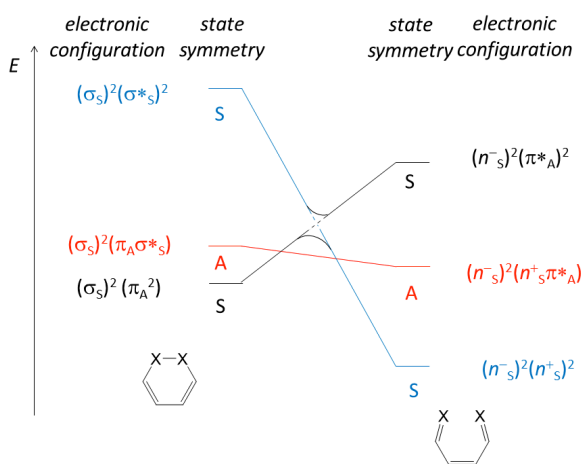


Figure 4. State correlation diagram for the orbitals involved in the ring opening of 1,2-dioxin and the related small models. The dashed line represents the diabatic curves while solid lines are used for the adiabatic representation. State symmetry labels are obtained by multiplying the symmetry of the orbitals with unpaired electrons according to the following rules: $S \times S = A \times A = S$, $S \times A = A \times S = A$; doubly occupied orbitals contribute with S.

Meanwhile, the $\sigma^*(S)$ antibonding orbital correlated with the corresponding symmetric combination of the lone pairs, $n_X(A)$.

Based on the symmetries of the orbitals and the transformations from the reactant to the product side, a state

S12. As can be seen in Fig. 3, the $\sigma(S)$ bonding orbital of the cyclic reactant correlates with the asymmetric combination of the lone pairs of X, $n_X(S)$, at the open structure in the product site. correlation diagram can be drawn, which illustrates the essence of the chemiexcitation process in a simple manner (Fig. 4; an analogous diagram for the in-plane ring opening is displayed in Fig. S13). The bond breaking brings a double crossing between the ground state and the lowest-lying excited state which belong to different symmetries (S and A, respectively) and therefore, without avoiding crossings. Considering the CASPT2//CASSCF reaction path calculations on 1,2-dioxin and the related models, the lowest-lying excited states becomes degenerated with the ground state in these molecules exactly at the TS region, therefore a single crossing rather than two crossings (as shown in Fig. 4) is found. At this crossing the nature or electronic configuration of the state can change from π_S^2 to $\pi_A \sigma_S^*$ or σ_S^* (black, red, and blue curves, respectively, in Fig. 4).

According to the analyses of the orbital and state correlation diagrams and the CASPT2 results for the ring opening of 1,2-dioxin, an important aspect to bring the chemiexcitation properties is the π -conjugation pattern close to the peroxide bond. Eight π electrons of 1,2-dioxin (four from the CC double bonds and four from the out-of-plane lone pairs of the OO) give rise to six π electrons plus two in-plane electrons in the di-carbonyl product. This conjugation pattern is achieved in the oxygenation step of L^2 . Furthermore, besides such aspect, the chemiexcitation efficiency of the -O-O- bond as compared to that of -S-S-, -NH-NH-, and -N-N- is also another crucial factor. Thus, the simplified description of the chemiexcitation displayed in Figs. 3 and 4 is in principle valid for the four isoelectronic systems. However, the thermochemistry and kinetics changes significantly. Table 1 compiles the results obtained for the activation energy barrier (ΔE^\ddagger) and the energy difference between product and reactant (ΔE) for the four models (Figs. S15-S18 displays the corresponding reaction paths). As can be seen, in all cases, the ground and excited states become energetically degenerate around the TS, which indicates that all the molecules are intrinsically chemiluminophores. However, only the peroxide bond breaking is kinetically and thermodynamically favorable. Dissociation of the -NH-NH-, and -N-N- bonds require a large energy barrier and the products are not significantly more stable than the reactants. This indicates that other changes of luminol rather than oxygenation to give the conjugated structure of the small models based on nitrogen would produce still chemiluminophores although much less efficient in comparison to CP^2 . Regarding the 1,2-dithiin model, it is worth noting that the reaction process is not any more exothermic. Nevertheless, the higher stability of the reactant as compared to the product suggests that it could be the basis for the design of a reversible chemiluminescent system. The derived conclusions (i.e. that among the considered bonds the peroxide bond provides the best conditions for efficient chemiexcitation) are in agreement with previous considerations by McCapra [Dani, ref 17].

For the CP^2 to $3AP^2$ transformation, a Walsh-like diagram based on CASSCF natural orbitals (see Fig. S19) keeps essentially the same chemiexcitation pattern as for the OO small

model. Among the highest occupied and lowest occupied orbitals of the product, it is possible to distinguish orbitals mainly belonging to the aniline moiety and others to the two carboxylate groups. As for 1,2-dioxin, the occupied n_{X} orbital of **3AP**⁻² correlates with an antibonding orbital in **CP**⁻² (σ^*) and the unoccupied $\pi_{3\text{AP}}^*$ orbital of the product is occupied in the reactant (π_{CP}).

Table 1. Energy differences (in kcal/mol) between products and reactants (ΔE) and activation energy barriers (ΔE^\ddagger) for the ring opening reaction of 1,2-dioxin (-O-O-), 1,2-dithiin (-S-S-) and the analogous compounds with the -NH-NH- and -N⁻-N⁻- bonds.

	ΔE	ΔE^\ddagger
-O-O-	-59.7	11.1
-S-S-	19.1	34.5
-NH-NH-	-12.2	36.7
-N ⁻ -N ⁻ -	-30.7	27.0

Chemiexcitation mechanism of **CP**⁻²

Going beyond Walsh diagram analyses, mapping of the PEHs for the ground and excited states along the OO bond dissociation of **CP**⁻² with the CASSCF/CASPT2 method shall allow to decipher the details of the mechanism. Fig. 5 illustrates the main results obtained from those multiconfigurational quantum-chemistry studies. Initial determinations of the key structures and reaction paths involved in the process were carried out by means of both the CASPT2//CASSCF and the CASPT2//CASPT2 protocols. At the **CP**⁻² equilibrium structure, hereafter $(\pi_{\text{CP}}^2)_{\text{min}}$, the nature of the ground state corresponds to a close-shell occupation of the π_{CP} orbital and the Mulliken charges indicate that the two electrons of the dianion are split between the carbonyl and peroxide groups on one side ($\delta=-1.2$) and the aniline ring on the other side ($\delta=-0.7$) (Table S2). Meanwhile, the lowest-lying excited state is mainly characterized by a single excitation from the π_{CP} orbital to the σ^* antibonding orbital related to the OO peroxide bond, hereafter $\pi_{\text{CP}}\sigma^*$. By using CASSCF geometries, the TS related to the OO bond breaking can be found, as previously done by Griesbeck et al.,^[31] who reported an OO bond length of 1.711 Å at such TS. The authors also found a low-energy CI at a much longer OO bond distance (2.094 Å). Our analyses indicate that the degenerate states at this point are the singly-excited configuration $\pi_{\text{CP}}\sigma^*$ and a close-shell configuration in which both electrons have been transferred from the π_{CP} to the σ^* orbitals, that is, a σ^{*2} state. This CI shall be denoted $(\sigma^{*2}/\pi_{\text{CP}}\sigma^*)_{\text{CI}}$. In addition, much closer to the **CP**⁻² reactant (OO bond length of 1.884 Å), we also found a region of CI between the π_{CP}^2 and $\pi_{\text{CP}}\sigma^*$ states, hereafter $(\pi_{\text{CP}}^2/\pi_{\text{CP}}\sigma^*)_{\text{CI}}$. Such double-crossing pattern agrees with the electronic-structure changes estimated in the state correlation

diagram of Fig. 4. Regarding the energetics, as mentioned in the Computational Details section, large differential correlation effects appear in this system, especially in this region close to **CP**⁻² and $(\pi_{\text{CP}}^2/\pi_{\text{CP}}\sigma^*)_{\text{CI}}$. Thus, at the CASSCF $(\pi_{\text{CP}}^2/\pi_{\text{CP}}\sigma^*)_{\text{CI}}$ point, the CASPT2 energy gap between S_0 and S_1 is 1.28 eV. This implies that CASSCF geometries are not good enough for an accurate description and we therefore proceeded to perform explorations of the PEHs at the CASPT2 level.

As a common chemiluminescent cyclic peroxide and considering the results on 1,2-dioxin and previous theoretical results on luminol, we expect that the molecule will easily undergo a thermally activated OO bond breaking, leading to the population of the excited manifold thought accessible CIs. In order to assess such possibility with the strongly correlated CASPT2 method, from the $(\pi_{\text{CP}}^2)_{\text{min}}$ minimum, we performed an energy grid exploration considering the fact that internal coordinates directly or indirectly involving OO bond stretching promote the system to the TS of the decomposition reaction and also produce a large energy decrease between the ground π_{CP}^2 and excited $\pi_{\text{CP}}\sigma^*$ states. Based on such exploration bending of the C10C2C3 and C11C3C2 angles and C10C2C3C11 dihedral twisting are here hypothesized as the most energetically accessible geometrical deformations leading to the breaking of the OO bond as well as the excited state population. These hypotheses are based on the geometrical analyses of the reaction path of 1,2-dioxin (Fig. S15), in which the mentioned internal coordinates are those which more significantly increases from the reactant to the TS/CI. For **CP**⁻², upon increasing the C10C2C3 and C11C3C2 angles from their values at the $(\pi_{\text{CP}}^2)_{\text{min}}$ point of 120.1 and 119.8°, respectively (which corresponds to an OO bond length of 1.508 Å), the π_{CP}^2 and $\pi_{\text{CP}}\sigma^*$ states exchange their energy ordering and the $\pi_{\text{CP}}\sigma^*$ state becomes the S_0 state (see Fig. S22). At an increase of 2°, which is related to an OO bond length of 1.636 Å, a CI at the CASPT2 level, hereafter $(\pi_{\text{CP}}^2/\pi_{\text{CP}}\sigma^*)_{\text{CI}}$, is identified and placed energetically only 0.13 eV above the $(\pi_{\text{CP}}^2)_{\text{min}}$ equilibrium geometry. This CI allows the population of the $\pi_{\text{CP}}\sigma^*$ state from the $(\pi_{\text{CP}}^2)_{\text{min}}$ ground state. Such bending of 2° was also found in 1,2-dioxin to reach the TS/CI point. Similar findings are obtained by exploring the C10C2C3C11 dihedral twisting (see Fig. S23), although requiring larger distortions.

From $(\pi_{\text{CP}}^2/\pi_{\text{CP}}\sigma^*)_{\text{CI}}$, CASPT2 minimum energy path (MEP) computations on the excited S_1 state do not exit the CI region, which might indicate that the shape of the CI is peaked and there is a local small energy barrier on the excited state. On the other hand, upon further increasing the C10C2C3 and C11C3C2 angles, the state related to the double excitation configuration, σ^{*2} , becomes substantially stabilized, and at C10C2C3 and C11C3C2 values of 131.1 and 130.8°, respectively, with an OO bond length of 2.298 Å, it becomes degenerated in energy with the $\pi_{\text{CP}}\sigma^*$ state (see Fig. S22). Such high-energy CI (HECI) point, hereafter $(\sigma^{*2}/\pi_{\text{CP}}\sigma^*)_{\text{HECI}}$, corresponds to a high-energy crossing in the seam of the $\sigma^{*2}/\pi_{\text{CP}}\sigma^*$ conical intersection. Regarding the energetics, according to the PEH mapping, energy barriers higher than 0.4 eV would be needed to populate the σ^{*2} PEH along the path from the $(\pi_{\text{CP}}^2/\pi_{\text{CP}}\sigma^*)_{\text{CI}}$ point. However, despite the latter

significant value, it is worth noticing that the $(\sigma^{*2}/\pi_{CP}\sigma^*)_{HECI}$ point is placed 0.96 eV below the $(\pi_{CP}^2/\pi_{CP}\sigma^*)_{CI}$, for which it is possible to presume that the system would be able to surmount the described barrier and reach the corresponding region.

By following the seam of the $(\sigma^{*2}/\pi_{CP}\sigma^*)_{HECI}$ with CASPT2 CI optimization computations, a low-energy CI region is reached, denoted as $(\sigma^{*2}/\pi_{CP}\sigma^*)_{CI}$, which has a relative energy of -2.4 eV and it is characterized by an OO bond distance of 2.001 Å. From

WILEY-VCH

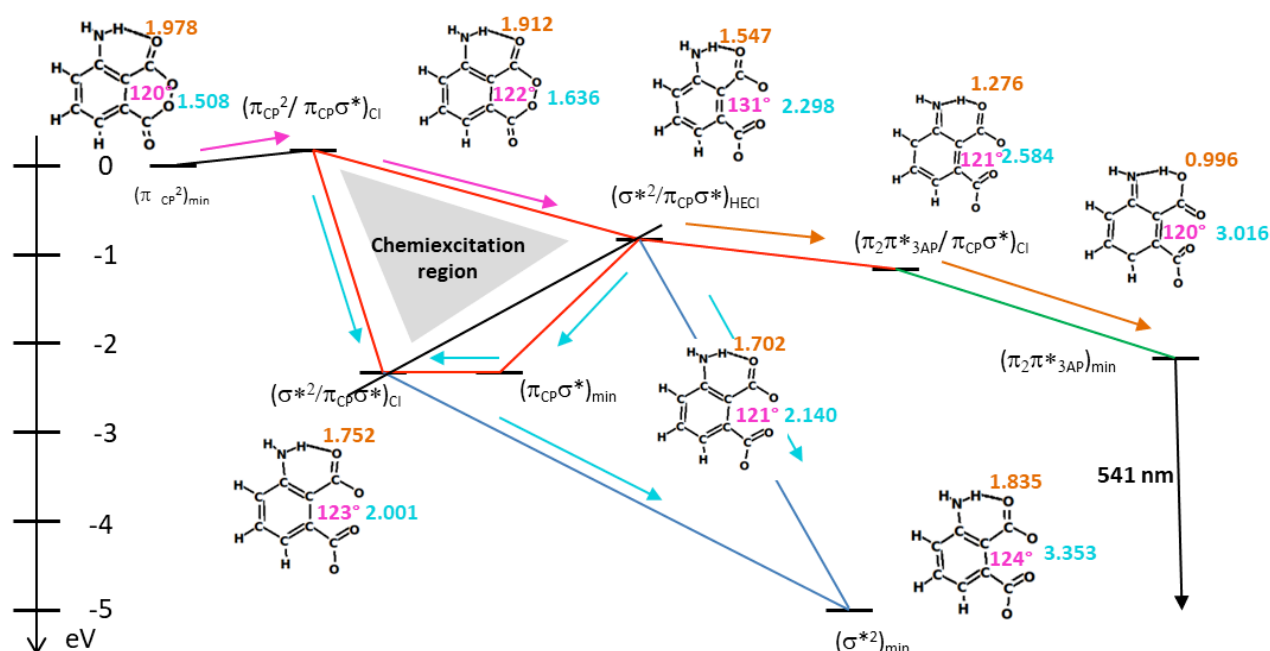


Figure 5. CASPT2/ANO-L-VDZP energy profiles for the radiative and non-radiative decomposition of CP^2 into 3AP^2 . Black, red, blue, and green solid lines indicate the evolution of the system on the π_{CP^2} , $\pi_{\text{CP}\sigma^*}$, σ^{*2} , $\pi_2\pi^*_{3\text{AP}}$ states, respectively. Purple, orange, and cyan arrows indicate that the main coordinate changing is the C10C2C3/C11C3C2 angles, the O13H16 bond length, and the O12O17 bond distance, respectively. The C10C2C3 angle (in degrees) and the O13H16 and O12O17 bond lengths (in Å) are also reported. See the SI for further data on the energetics (Table S1 and Figs. S22–S29), geometries (Figs. S20–S21), and Mulliken charges (Table S2).

this point, CASPT2 MEP computations on the $\pi_{\text{CP}\sigma^*}$ state produce new converged points along the excited surface (see Fig. S24), which contrasts with the failed attempts to exit the $(\pi_{\text{CP}^2}/\pi_{\text{CP}\sigma^*})_{\text{Cl}}$ region by MEP computations. This indicates that the $(\sigma^{*2}/\pi_{\text{CP}\sigma^*})_{\text{Cl}}$ has in this case a sloped shape (see Fig. 5).

CP^2 can reach $(\sigma^{*2}/\pi_{\text{CP}\sigma^*})_{\text{Cl}}$ from the previous $(\pi_{\text{CP}^2}/\pi_{\text{CP}\sigma^*})_{\text{Cl}}$ crossing along the ground state PEH as can be seen from the energy profile displayed in Figs. 5 and S25. This scenario corresponds to the drawings based on Walsh diagrams (Fig. 4) and differ from the findings obtained in 1,2-dioxin (Fig. S15). The reason can be attributed to the fact that in CP^2 the $\pi_{\text{CP}\sigma^*}$ state is stabilized by electron donation from the aniline moiety producing then two regions of crossing rather than one in 1,2-dioxin. The involvement of an intramolecular electron transfer towards the peroxide bond in the chemiexcitation mechanism is not new, and in fact constitutes the first step of the so-call "Chemically Initiated Electron Exchange Luminescence (CIEEL)" mechanism [Dani, ref 14], proposed as a general chemiluminescence mechanism in peroxide-contained systems. An intramolecular electron transfer has in fact been proposed to operate in various 1,2-dioxetanes systems containing phenolate or acridinium substituents [Dani, ref 15,16]. Such stabilization was also theoretically described recently in the intermolecular chemiluminescence mechanisms

activated by aromatic compounds with low ionization potential.^[1,39] In between $(\pi_{\text{CP}^2}/\pi_{\text{CP}\sigma^*})_{\text{Cl}}$ and $(\sigma^{*2}/\pi_{\text{CP}\sigma^*})_{\text{Cl}}$, the ground and excited states PEHs do not show a high energy gap, which indicates that the points between $(\pi_{\text{CP}^2}/\pi_{\text{CP}\sigma^*})_{\text{Cl}}$ and $(\sigma^{*2}/\pi_{\text{CP}\sigma^*})_{\text{Cl}}$ can be considered as the chemiexcitation region. According to the obtained $(\pi_{\text{CP}^2}/\pi_{\text{CP}\sigma^*})_{\text{Cl}}$ and $(\sigma^{*2}/\pi_{\text{CP}\sigma^*})_{\text{Cl}}$ structures, at OO bond lengths shorter than ~ 1.6 Å, the $\pi_{\text{CP}\sigma^*}$ state corresponds to S_1 , it becomes S_0 in the range $\sim 1.6 - 2.0$ Å, and at larger distances it is again the excited S_1 state. Considering such geometrical analyses, it can be stated that those molecules accessing the chemiexcitation region with high kinetic energy at the C10C2C3 and C11C3C2 angles shall reach S_1 at high-energy crossing points such as $(\sigma^{*2}/\pi_{\text{CP}\sigma^*})_{\text{HECl}}$. Otherwise, the system is expected to vibrationally relax along the S_0 in the chemiexcitation region and access the excited PEH at closer structures to the $(\sigma^{*2}/\pi_{\text{CP}\sigma^*})_{\text{Cl}}$.

Summarizing, the chemiexcitation mechanism of CP^2 pass to a easily thermally activated OO bond breaking, mostly involving the elongation of the C10C2C3 and C11C3C2 angles. Such a process determines a substantial stabilization of the $\pi_{\text{CP}\sigma^*}$ and σ^{*2} states, consequently leading to accessible conical intersections among the π_{CP^2} , $\pi_{\text{CP}\sigma^*}$ and σ^{*2} roots, which in turns constitute the gates for the population of the excited manifold of the system.

Light emission

Three types of points characterizes the chemiexcitation region, $(\pi_{CP}^2/\pi_{CP}\sigma^*)_{CI}$, $(\sigma^{*2}/\pi_{CP}\sigma^*)_{HECI}$, and $(\sigma^{*2}/\pi_{CP}\sigma^*)_{CI}$ (see Fig. 5). As mentioned above, the excited state (S_1) evolution from the first structure present energy barriers which might be attributed to a peaked nature of the CI. On the other hand, CASPT2 MEP computations from $(\sigma^{*2}/\pi_{CP}\sigma^*)_{CI}$ give rise to an evolution toward the equilibrium structure of the $\pi_{CP}\sigma^*$ state, denoted as $(\pi_{CP}\sigma^*)_{min}$, with a relative energy of -2.45 eV and an OO bond length of 2.140 Å (see Figs. 5 and S24). As compared to $(\pi_{CP}^2)_{min}$, $(\pi_{CP}\sigma^*)_{min}$ has a higher net charge in the carboxylate groups ($\delta=-1.8$), which is the consequence of the electron promotion from the aniline ring to the peroxide bond (see Table S2), a process reminding the intramolecular electron transfer characterizing the CIEEL mechanism [Dani, ref 14]. Focusing on the nomenclature of the product (**3AP**²) orbitals, this state can be also referred as a $n_{O-\pi_{3AP}}\sigma^*$ electronic transition (see Fig. S19). Only a small energy relaxation of 0.05 eV takes place. At this relaxed point, the S_0 state is relatively close in energy, being separated by 0.52 eV from S_1 . Based on both results, it can be concluded that radiative decay is not a favorable process in this region. The $(\sigma^{*2}/\pi_{CP}\sigma^*)_{CI}$ structure, which funnels the energy to the ground state σ^{*2} PEH is isoenergetic, therefore, radiationless decay rate is expected to be very high. In fact, this structure can be associated to the non-emissive $n\pi^*$ excited state minimum located in the dioxetanone-based chemiluminescence molecules.^[40,41] In the present work, to determine the non-radiative decay path, numerical CASPT2 MEP computations were carried out on the σ^{*2} state from the $(\sigma^{*2}/\pi_{CP}\sigma^*)_{CI}$, which evolves towards its corresponding minimum, $(\sigma^{*2})_{min}$, placed at a relative energy of -5.17 eV with respect to the reactant $(\pi_{CP}^2)_{min}$, and corresponding to the **3AP**² product of the chemiluminescence reaction (see Fig. S26). Geometrically, the minimum is characterized by an OO bond length of 3.353 Å and a significant rotation of both the amino and the carboxylate groups (see Figs. S20-S21). As can be seen from the analysis of the Mulliken charges (Table S2), the two extra electrons are fully located in the COO groups.

From the third representative crossing in the chemiexcitation region, $(\sigma^{*2}/\pi_{CP}\sigma^*)_{HECI}$, CASPT2 MEP calculations on the excited state $\pi_{CP}\sigma^*$ (or $n_{O-\pi_{3AP}}\sigma^*$) give rise to an evolution towards the non-emissive $(\pi_{CP}\sigma^*)_{min}$ structure (see Fig. S27), which as mentioned above decays in a radiationless manner via $(\sigma^{*2}/\pi_{CP}\sigma^*)_{CI}$. MEP computations on the σ^{*2} state from $(\sigma^{*2}/\pi_{CP}\sigma^*)_{HECI}$ (see Fig. S26) also produces the $(\sigma^{*2})_{min}$ equilibrium structure of **3AP**².

The experimentally recorded chemiluminescence maxima of luminol in DMSO is equal to 485-510^[18-21] nm (2.43-2.55 eV). The characterized $(\pi_{CP}\sigma^*)_{min}$, placed only 0.52 eV above S_0 , cannot consequently be the species accounting for the recorded chemiluminescent emission, which further supports the predicted radiationless decay for the $\pi_{CP}\sigma^*$ state via $(\sigma^{*2}/\pi_{CP}\sigma^*)_{CI}$. To search for the light emitter, the photochemical reaction path of the **3AP**² product on the lowest-lying excited state of $\pi_2\pi_{3AP}\sigma^*$ nature was determined by performing MEP computations with both the CASPT2//CASSCF and CASPT2 protocols (Fig. S28). As for the findings obtained for the

chemiexcitation mechanism, the chemistry of $\pi_2\pi_{3AP}\sigma^*$ is also largely affected by differential correlation. Thus, CASSCF stops at a structure denoted as $(\pi_2\pi_{3AP}\sigma^*)_{CASSCF}$ with a very large CASPT2//CASSCF vertical emission energy (3.70 eV) far from the experimental value. In contrast, along the CASPT2 MEP, an excited state proton transfer from the amino group to the nearby carboxylate group takes place, producing an equilibrium structure [hereafter, $(\pi_2\pi_{3AP}\sigma^*)_{min}$] with a vertical emission energy of 2.29 eV, which is now in reasonably good agreement with the experimental data.^[18-21] This supports previous experimental suggestions on the chemical nature of the light emitter in DMSO.^[18] Our analyses also indicate that the negative charge located in the carboxylate group nearby the amino moiety in the $(\sigma^{*2})_{min}$ is now split into both the carboxylate and the amino groups ($\delta=-0.2$ and -0.6 , respectively), see Fig. 5 and Table S2. In order to evaluate the ability of the system to reach the $(\pi_2\pi_{3AP}\sigma^*)_{min}$ light emitter from the chemiexcitation region, the PEH of the ground and excited states between the $(\sigma^{*2}/\pi_{CP}\sigma^*)_{HECI}$ and $(\pi_2\pi_{3AP}\sigma^*)_{min}$ structures and between the $(\pi_{CP}\sigma^*)_{min}$ and $(\pi_2\pi_{3AP}\sigma^*)_{min}$ geometries were mapped at the CASPT2 level (see Fig. S29). The $(\pi_2\pi_{3AP}\sigma^*)_{min}$ emitter is located at a relative energy of -2.21 eV in between the energies of the two CIs and slightly above the energy of the non-emissive $(\pi_{CP}\sigma^*)_{min}$. Energy mapping from both $(\pi_{CP}\sigma^*)_{min}$ and $(\sigma^{*2}/\pi_{CP}\sigma^*)_{HECI}$ points shows that the system must cross an additional CI denoted as $(\pi_2\pi_{3AP}\sigma^*/\pi_{CP}\sigma^*)_{CI}$ placed at -1.29 eV. It is expected that the molecules reaching $(\sigma^{*2}/\pi_{CP}\sigma^*)_{HECI}$, with some kinetic energy content at the C10C2C3 bending mode should favor the evolution towards $(\pi_2\pi_{3AP}\sigma^*)_{min}$ due to the decrease in the hydrogen bond length between the amino and carboxylate groups provided by such vibrational mode.

Having characterized the chemiluminescence mechanism on the singlet manifold, it is worth evaluating a possible contribution of the triplet states. Although it has been proven that luminol chemiluminescence emission is originated as fluorescence radiation [18-20] (i.e. from a singlet state) a relaxation into the triplet state can however be important, providing a competing relaxation path affecting the global chemiluminescence quantum yield. In order to assess the involvement of the triplet states, the low-lying triplet states at the characterized critical points reported in Figure 5 have been computed. The corresponding energies are reported in Table S4. As it can be seen the T1 state is below the π_{CP}^2 and $\pi_{CP}\sigma^*$ states at the $(\pi_{CP}^2/\pi_{CP}\sigma^*)_{CI}$ conical intersection. The nature of such T1 state is of a triplet $\pi_{CP}\sigma^*$ state, and will then thereafter label as $^3\pi_{CP}\sigma^*$. The same triplet state is at the $(\pi_{CP}^2)_{min}$ geometry the T2 states, placed energetically in between the π_{CP}^2 and $\pi_{CP}\sigma^*$ states. Such a result points out to a crossing between the singlet π_{CP}^2 root and the $^3\pi_{CP}\sigma^*$ state along the reaction path connecting the two mentioned geometries. In order to evaluate the importance of a possible decay into the $^3\pi_{CP}\sigma^*$ state, the spin-orbit coupling of the latter with the π_{CP}^2 state has been computed at both the $(\pi_{CP}^2)_{min}$ and $(\pi_{CP}^2/\pi_{CP}\sigma^*)_{CI}$ geometries. Non-negligible SOCs values have been obtained (13.61 and 10.91 cm^{-1} at the $(\pi_{CP}^2)_{min}$ and $(\pi_{CP}^2/\pi_{CP}\sigma^*)_{CI}$ geometries, respectively) which are compatible with a possible decay into the triplet manifold. However such an intersystem crossing process is in direct

competition with an internal conversion to the singlet $\pi_{CP}\sigma^*$ state, occurring in the same part of the system PEHs. It is then plausible to suppose that, due to the significant but still not particularly high SOCs values and the competition with a non-spin forbidden decay path (i.e. population of the $\pi_{CP}\sigma^*$ state), the relaxation into the triplet manifold constitute a minor route in the present system, probably leading to a small reduction in the chemiluminescence quantum yield, but not directly involved in the emission process. The $(\pi_2\pi_{3AP}^*/\pi_{CP}\sigma^*)_{CI}$ structure is also characterized by a similar near singlet-triplet energy degeneracy, being the T2 $^3\pi_{CP}\sigma^*$ state 0.07 and 0.09 eV below the $\pi_2\pi_{3AP}^*$ and $\pi_{CP}\sigma^*$ states, respectively. The computed SOCs values accounting for such interactions are equal to 3.78 and 6.35 cm^{-1} , so again is reasonable to assume that only a small fraction of the excited state population will decay into the triplet manifold.

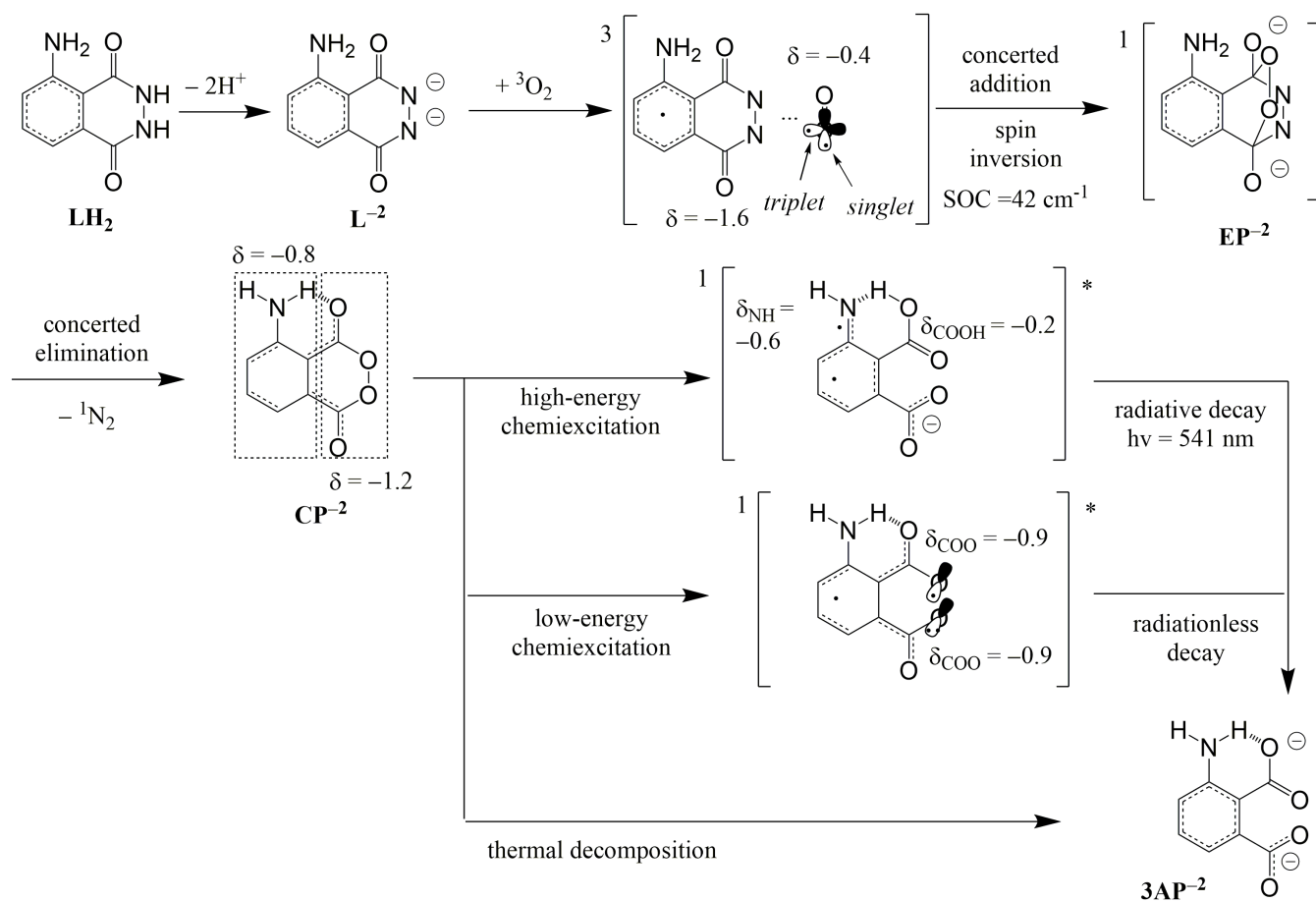
Summary and conclusions

The molecular basis of the chemiluminescence mechanism of luminol were determined in this work by means of reaction path computations and PEH mappings with DFT and the strongly-correlated CASPT2 method and by focusing separately on the three relevant steps of the process, (i) the generation of the chemiluminophore from the luminol, (ii) the chemiexcitation, and (iii) the production of light emission. The findings allow to improve the conventional mechanism^[15,22] and provide novel information on the unexplored parts of the process, giving rise to the scheme displayed in Scheme 2.

For the first step, the addition of oxygen to the molecule was found to require a double deprotonation of luminol (LH_2) to generate the dianion (L^{2-}). A single electron transfer from L^{2-} to $^3\text{O}_2$ rather than the proposed double electron transfer takes place. Such step is crucial to overcome the intrinsically forbidden population transfer from the triplet to the singlet manifold. Also, in contrast to previous suggestions, the addition occurs in a concerted manner rather than a stepwise process, giving rise to the bicyclic intermediate EP^{2-} . Finally, the chemiluminophore CP^{2-} is produced after $^1\text{N}_2$ elimination in a concerted process. Such a mechanism should be the one operating in organic solvents

Subsequently, to comprehend the next step related to the chemiexcitation of CP^{2-} , we firstly determined the factors which allows to rationalize the requirement of oxygen incorporation in LH_2 . The -O-O-, -NH-NH-, -N-N-, and -S-S- chemical functionalities were found to have in all cases properties for chemiexcitation, however, -O-O- (and therefore CP^{2-}) is the only case in which the decomposition and excited state population is both kinetically and thermodynamically efficient. Furthermore, the 1,2-dioxin chemical functionality is proposed here to be useful for rapid chemiexcitation and short chemiluminescence lifetimes, which is shall be relevant for the design of ultrasensitive chemiluminescence assays. The chemiluminophore properties were next confirmed by analyzing the chemiexcitation process in the CP^{2-} molecule. For such process the strongly-correlated CASPT2 method was found to be needed for both geometry and energy determinations. Based on the obtained results, the following mechanism is proposed

accounting for the chemiexcitation. From the CP^{2-} equilibrium structure, with a π_{CP}^{2-} nature, an electron transfer from the π conjugated system of the aniline moiety to the anti-bonding σ^*



Scheme 2. Reaction mechanism of ${}^3\text{O}_2 + \text{L}^{-2} \rightarrow \text{CP}^{-2} + {}^1\text{N}_2$, showing the chemiluminescence route (a), radiationless decay (b), and the thermal decomposition path (c), and displaying the main geometrical and electronic-structure properties determined in this work with the DFT and CASPT2 methods (see text).

orbital of the OO bond activates the decomposition process, which is characterized by a small energy barrier of 0.13 eV. Such an electron transfer characterizing the chemiexcitation mechanism remind the first step of the so-call CIEEL mechanism, accordingly to which chemiluminescence of peroxide containing systems, as various 1,2-dioxetanes systems containing phenolate or acridinium substituents, is initially triggered by an intramolecular electron transfer toward the O-O bond [Dani, ref 14-16]. The OO bond breaking also brings the system to the $(\pi_{\text{CP}}^2/\pi_{\text{CP}}\sigma^*)_{\text{Cl}}$ crossing at an OO bond length of 1.6 Å. The system access at this point a region in which the energy gap between the ground and excited states is not significantly high, the chemiexcitation region. Such region finishes upon further increasing 0.4-0.7 Å the OO bond distance, when the electronic configuration with two electrons transferred to the σ^* orbitals is more stable than the configuration with only one electron transferred. The chemiexcitation region is characterized by a reorganization of the single and double bonds in the molecule, where the six-member ring becomes aromatic. Along the chemiexcitation region, a seam of crossings between the $\pi_{\text{CP}}\sigma^*$ and σ^{*2} states is found, with two

representative CIs, one at high energies, $(\sigma^{*2}/\pi_{\text{CP}}\sigma^*)_{\text{HECI}}$, and the other at the low-energy region of the seam, $(\sigma^{*2}/\pi_{\text{CP}}\sigma^*)_{\text{Cl}}$. From such degeneracy region, the molecule can either relax on the σ^{*2} state reaching the *thermal decomposition* (3AP^{-2}) or continue the excited state $\pi_{\text{CP}}\sigma^*$. $(\sigma^{*2}/\pi_{\text{CP}}\sigma^*)_{\text{HECI}}$ can be considered as a representative structure to populate the excited state for those molecules with high kinetic energy at the bending internal coordinates related to the separation of the carboxylate groups, specially the bending of the carboxylate group nearby the amino group. Meanwhile, $(\sigma^{*2}/\pi_{\text{CP}}\sigma^*)_{\text{Cl}}$ represents a low-kinetic energy evolution along the chemiexcitation region.

After excited state population at the chemiexcitation part of the PEHs from either the HECI or the low-energy CI, the steepest descendent evolution is towards the equilibrium structure of the $\pi_{\text{CP}}\sigma^*$ excited state. Such minimum is however isoenergetic and close to σ^{*2} . Therefore, *radiationless decay* to the ground state is expected for this route. On the other hand, if the system continues increasing the angles related to the OO bond stretching and approaching the amino and carboxylate groups, a proton transfer is feasible, which implies a $\pi_{\text{CP}}\sigma^*$ to $\pi_2\pi_{3\text{AP}}^*$ excited state population transfer and the formation of the

light emitter species. This emitter which relax by *radiative decay* with a vertical emission energy equal to 2.29 eV (541 nm), in agreement with the experimental chemiluminescence maxima of luminol in DMSO, equal to 485^[18]/502^[19,20]/510^[21] nm in DMSO.

In different part of the text a mention to the so call CIEEL mechanism has been made, which is a general chemiluminescence mechanism proposed to occurs in peroxide-containing systems [Dani, ref 14]. Accordingly to CIEEL, chemiluminescence in peroxide-containing system involved two main steps: an electron transfers from an intra- or inter-molecular activator to the peroxidic bond; a back-transfer form the broken peroxidic bond back to the activator, which is then promoted to its excited manifold from which emission can be generated. Accordingly to our results, in the chemiluminescence process undertaken by CP-2, a CIEEL-like mechanism is indeed described, where the aniline structure acts as activator. As show in table S2 and more specifically in table S3, a 0.6 electron transfer is described from the aniline to the remaining part of the molecule (C10O13O17C11O12O18 atoms) from the $(\pi_{CP}\sigma^*)_{min}$ to the $(\sigma^{*2}/\pi_{CP}\sigma^*)_{HECl}$ geometry, while a 0.4 back electron transfer is described form the $(\sigma^{*2}/\pi_{CP}\sigma^*)_{HECl}$ conical intersection to the emitting region. The latter value increase to a 0.7 electron transfer if considering the described hydrogen transfer (see Table S3). The general importance of the CIEEL mechanism is consequently here supported, being also relevant for the luminol chemiluminescence process.

Overall, the path leading to the chemiluminescent emission is here described as a possible route but not as the most favorable decay taking place in the system, the latter being instead a non-radiative relaxation. Such a result can be understood in the light of the experimental chemiluminescent quantum yield in DMSO, of the order of 10^{-2} , which indicate that the chemiluminescent mechanism is not the most favorable process in the molecule. Nevertheless, in comparison to other dioxetane- and dioxetanone-based systems, luminol implies a more efficient singlet excited state population which can be related to both a very low energy barrier for the decomposition reaction and an appropriate shape of the chemiexcitation region. Thus, in the dioxetane and dioxetanone systems with lower efficiency, the near-degeneracy PEH region representing the OO and CC bond breakings is planar or takes place at the TS. On the contrary, in luminol, it takes place after the TS region and it is very steep which can be expected to favor the system to gain kinetic energy and by this means increase the probability for continuing the reactivity on the excited state. To increase the chemiluminescence yield, we propose that hot vibrational states mainly related to the bending of the C10C2C3 and C11C3C2 angles must be populated, which could be possible via selective activation with IR wavelengths. This type of radiation has much deeper tissue penetration as compared to the UVA light used in photodynamic therapy and therefore, this would help to treat tumors not accessible to the UVA-induced techniques.

Computational Section

The DFT and CASSCF/CASPT2^[42-44] methods were used in this work as implemented in the Gaussian 09^[45] and MOLCAS 8^[46] programs, respectively, to decipher the molecular basis of the chemiluminescence mechanism of luminol. All computations were carried out by imposing no restrictions to the symmetry of the molecule (C_1 symmetry). The long-range corrected BLYP functional (LC-BLYP)^[47-50] was used with the 6-31G* basis set, hereafter LC-BLYP/6-31G*, to determine the minima and TS for the $L^{-2} + {}^3O_2 \rightarrow CP^{-2}$ reaction step. The open-shell approach, as established in previous studies,^{[32,33, Dani, ref 1,2,3,4,5,6],^[32,33]} was used to correctly determine the geometries and energies of the singlet biradical structures. The reaction vector at the TS was analyzed to confirm the connectivity between reactants and products. The energy profile obtained was confirmed by energy calculation using other DFT levels of theory, LC-BLYP/6-311++G(2df,2dp), CAM-B3LYP/6-31G*,^[51] and LC-BLYP/6-31G* with the polarizable continuum model (PCM) for DMSO.^[45]

The CASSCF/CASPT2 method was used (i) to study the oxygenation of L^{-2} , (ii) to analyze the chemiexcitation efficiency of 1,2-dioxin (see Scheme 1) and its analogous models with the -N-N-, -NH-NH-, and -S-S- bonds rather than -O-O-, and (iii) to determine the chemiexcitation and light emission mechanism of CP^{-2} . The CASPT2//DFT protocol (i.e. single point CASPT2 computations on top of DFT optimized geometries) was used in (i) with a basis set of atomic natural orbitals (ANO) of S-type^[52] contracted to C,N,O[3s,2p,1d]/H[2s1p], hereafter ANO-S-VDZP. For (ii), the CASPT2//CASSCF protocol was used with VDZP ANO basis set of L-type (ANO-L-VDZP).^[53,54] For (iii), such protocol was also initially considered, although it was shown to give rise to strong differential correlation problems and then the CASPT2//CASPT2 protocol was finally used with the ANO-S-VDZP basis set. In this last protocol, the required gradients were evaluated numerically. The CASPT2 zeroth-order Hamiltonian was employed as originally implemented by setting the ionization-potential electron-affinity parameter to 0.00 au^[55] and the core orbitals were frozen in the all CASPT2 calculations. An imaginary level shift of 0.20 au was used to minimize the effect of weakly-interacting intruder states.^[56] Such CASPT2 approach has been validated during the last decades in many different studies on organic molecules.^[57-61] For (ii) a highly-correlated active space of 10 electrons distributed among 8 orbitals [CAS(10,8)] was used and corresponds to all relevant valence σ , σ^* , n , π , and π^* orbitals (see Figs. S1-S4). Four singlet and four triplet CASSCF wave functions were averaged in such computations to take into account the possibility of appearing distinct biradical configurations as in 1,2-dioxetane^[1,62,63] or Dewar dioxetane.^[64] Based on the analyses on the 1,2-dioxin small model and further tests on the luminol system, for (i) and (iii), an appropriate CAS(12,10) was chosen for geometry optimizations and a CAS(18,14) for single point CASPT2 computations (see Figs. S5-S8). CASSCF state-averaging over a different number of roots was performed accordingly to the type of computation, four for single point calculations and two for geometry optimizations.

The energy mapping of the potential energy hypersurfaces (PEHs) was achieved by minimum energy path (MEP) calculations^[65] or geometry optimizations of minima and CI searches^[65] combined by linear interpolation of internal coordinate (LIIC) calculations. CASSCF CIs were determined by using the restricted Lagrange multipliers technique as included in the MOLCAS 8 package^[46] in which the lowest-energy point is obtained under the restriction of degeneracy between the two considered states.^[65] CASPT2 CIs were searched by extended grid explorations using the gradients of the CASSCF CI computations, as described elsewhere.^[66,67]

Spin-orbit coupling (SOC) was computed in (i) at the CASSCF/CASPT2 level by means of the complete-active-space state-interaction with spin-orbit method^[68] using the atomic mean field approximation.^[69] Corrections for the basis set superposition error

(BSSE) were also calculated for the CASPT2 energetics of (i) by using the counterpoise correction (CP).^[70,71]

Acknowledgements

This work has received financial support by the Spanish MICINN (projects CTQ2017-87054-C2-2-P; "Ramón y Cajal" grant RYC-2015-19234; Unidad de Excelencia María de Maetzu MDM-2015-0538), the Generalitat Valenciana (PROMETEO/2016/135), and the Swedish Research Council (grant 2016-033989).

Author contributions

D.R.-S. and R.L. conceived the study. A.G., M.L., and D.R.-S. performed the computations of the oxygenation step. P.F. and D.M.-M., and D.R.-S. performed the computations on the small models. A.G. performed the calculations of the chemiexcitation and light-emission mechanism. All authors analysed and interpreted all the results and contributed to paper writing.

Notes

‡ CASPT2 energies are computed on top of optimized CASSCF geometries for 1,2-dioxin and the analogues rather than full CASPT2 determinations because no significant differential correlation effects are detected in these cases.

Keywords: luminol • chemiluminescence • chemiexcitation efficiency • CASPT2 • conical intersections

- [1] M. Vacher, I. Fdez Galván, B. W. Ding, S. Schramm, R. Berraud-Pache, P. Naumov, N. Ferré, Y. J. Liu, I. Navizet, D. Roca-Sanjuán, et al., *Chem. Rev.* **2018**, *118*, 6927–6974.
- [2] F. H. Bartoloni, L. F. M. L. Ciscato, M. M. de M. Peixoto, A. P. F. dos Santos, C. da S. Santos, S. de Oliveira, F. A. Augusto, A. P. E. Pagano, W. J. Baader, E. L. Bastos, *Quim. Nova* **2011**, *34*, 544–554.
- [3] H. O. Albrecht, *Z. Phys. Chem.* **1928**, *136*, 321–330.
- [4] X. Zhang, S. He, Z. Chen, Y. Huang, *J. Agric. Food Chem.* **2013**, *61*, 840–847.
- [5] W. R. Seitz, D. M. Hercules, *Anal. Chem.* **1972**, *44*, 2143–2149.
- [6] D. L. Giokas, D. C. Christodouleas, I. Vlachou, A. G. Vlessidis, A. C. Calokerinos, *Anal. Chim. Acta* **2013**, *764*, 70–77.
- [7] C. Dodeigne, L. Thunus, R. Lejeune, *Talanta* **2000**, *51*, 415–39.
- [8] D. W. O'Sullivan, A. K. Hanson, D. R. Kester, *Mar. Chem.* **1995**, *49*, 65–77.
- [9] M. Ma, F. Diao, X. Zheng, Z. Guo, *Anal. Bioanal. Chem.* **2012**, *404*, 585–592.
- [10] K. Berg, T. A. Theodossiou, "Lumiblast," can be found under <http://www.lumiblast.eu>, n.d.
- [11] H. Yuan, H. Chong, B. Wang, C. Zhu, L. Liu, Q. Yang, F. Lv, S. Wang, *J. Am. Chem. Soc.* **2012**, *134*, 13184–13187.
- [12] N. Yesilgul, T. B. Uyar, O. Seven, E. U. Akkaya, *ACS Omega* **2017**, *2*, 1367–1371.
- [13] Ł. Ożóg, J. Tabarkiewicz, D. Aebisher, *Eur. J. Clin. Exp. Med.* **2017**, *15*, 95–98.
- [14] C. M. Magalhães, J. C. G. Esteves da Silva, L. Pinto da Silva, *ChemPhysChem* **2016**, *17*, 2286–2294.
- [15] W. J. Baader, C. V. Stevani, E. L. Bastos, in *Chem. Peroxides* (Ed.: Z. Rappoport), John Wiley & Sons, Ltd, Chichester, UK, **2006**, pp. 1211–1278.
- [16] E. H. White, D. F. Roswell, *Acc. Chem. Res.* **1970**, *3*, 54–62.
- [17] F. McCapra, *Q. Rev. Chem. Soc.* **1966**, *20*, 485.
- [18] E. H. White, M. M. Bursley, *J. Am. Chem. Soc.* **1964**, *86*, 941–942.
- [19] J. Lind, G. Merenyi, T. E. Eriksen, *J. Am. Chem. Soc.* **1983**, *105*, 7655–7661.
- [20] D. F. Roswell, E. H. White, *Methods Enzymol.* **1978**, *57*, 409–423.
- [21] P. D. Wildes, E. H. White, *J. Am. Chem. Soc.* **1973**, *95*, 2610–2617.
- [22] F. A. Augusto, G. A. de Souza, S. P. de Souza Júnior, M. Khalid, W. J. Baader, *Photochem. Photobiol.* **2013**, *89*, 1299–1317.
- [23] J. Lee, H. H. Seliger, *Photochem. Photobiol.* **1972**, *15*, 227–237.
- [24] A. M. Garcia-Campana, W. R. G. Baeyens, L. Cuadros-Rodriguez, F. A. Barrero, J. M. B.-S. and L. Gamiz-Gracia, *Curr. Org. Chem.* **2002**, *6*, 1–20.

- [25] G. Merényi, J. Lind, T. E. Eriksen, *J. Biolumin. Chemilumin.* **1990**, *5*, 53–56.
- [26] Y. Omote, T. Miyake, N. Sugiyama, *Bull. Chem. Soc. Jpn.* **1967**, *40*, 2446–2448.
- [27] D. Kearns, S. Ehrenson, *J. Am. Chem. Soc.* **1962**, *84*, 739–742.
- [28] W. R. Seitz, *J. Phys. Chem.* **1975**, *79*, 101–106.
- [29] J. Michl, *Photochem. Photobiol.* **1977**, *25*, 141–154.
- [30] C. R. Flynn, J. Michl, *J. Am. Chem. Soc.* **1974**, *96*, 3280–3288.
- [31] A. G. Griesbeck, Y. Díaz-Miara, R. Fichtler, A. Jacobi Von Wangelin, R. Pérez-Ruiz, D. Sampedro, *Chem. - A Eur. J.* **2015**, *21*, 9975–9979.
- [32] L. P. Da Silva, J. C. G. E. Da Silva, *J. Comput. Chem.* **2012**, *33*, 2118–2123.
- [33] L. Yue, D. Roca-Sanjuán, R. Lindh, N. Ferré, Y. J. Liu, *J. Chem. Theory Comput.* **2012**, *8*, 4359–4363.
- [34] M. A. El-Sayed, *Acc. Chem. Res.* **1968**, *1*, 8–16.
- [35] R. Berraud-Pache, R. Lindh, I. Navizet, *J. Phys. Chem. B* **2018**, *122*, 5173–5182.
- [36] H. Kondo, T. Igarashi, S. Maki, H. Niwa, H. Ikeda, T. Hirano, *Tetrahedron Lett.* **2005**, *46*, 7701–7704.
- [37] B.-W. Ding, Y.-J. Liu, *J. Am. Chem. Soc.* **2017**, *139*, 1106–1119.
- [38] R. Prabhakar, P. E. M. Siegbahn, B. F. Minaev, H. Ågren, *J. Phys. Chem. B* **2002**, *106*, 3742–3750.
- [39] F. A. Augusto, A. Francés-Monerris, I. Fdez Galván, D. Roca-Sanjuán, E. L. Bastos, W. J. Baader, R. Lindh, *Phys. Chem. Chem. Phys.* **2017**, *19*, 3955–3962.
- [40] D. Roca-Sanjuán, M. G. Delcey, I. Navizet, N. Ferré, Y. J. Liu, R. Lindh, *J. Chem. Theory Comput.* **2011**, *7*, 4060–4069.
- [41] S. F. Chen, I. Navizet, D. Roca-Sanjuán, R. Lindh, Y. J. Liu, N. Ferré, *J. Chem. Theory Comput.* **2012**, *8*, 2796–2807.
- [42] K. Andersson, P. Å. Malmqvist, B. O. Roos, A. J. Sadlej, K. Wolinski, *J. Phys. Chem.* **1990**, *94*, 5483–5488.
- [43] D. Roca-Sanjuán, F. Aquilante, R. Lindh, *Wiley Interdiscip. Rev. Comput. Mol. Sci.* **2012**, *2*, 585–603.
- [44] K. Andersson, P. Malmqvist, B. O. Roos, *J. Chem. Phys.* **1992**, *96*, 1218–1226.
- [45] M. J. Frisch, G. W. Trucks, H. B. Schlegel, G. E. Scuseria, M. A. Robb, J. R. Cheeseman, G. Scalmani, V. Barone, B. Mennucci, G. A. Petersson, et al., *Gaussian Inc., Wallingford* **2013**, DOI 10.1016/j.chroma.2009.10.045.
- [46] F. Aquilante, J. Autschbach, R. K. Carlson, L. F. Chibotaru, M. G. Delcey, L. De Vico, I. Fdez. Galván, N. Ferré, L. M. Frutos, L. Gagliardi, et al., *J. Comput. Chem.* **2016**, *37*, 506–541.
- [47] H. Iikura, T. Tsuneda, T. Yanai, K. Hirao, *J. Chem. Phys.* **2001**, *115*, 3540–3544.
- [48] A. D. Becke, *Phys. Rev. A* **1988**, *38*, 3098–3100.
- [49] C. Lee, W. Yang, R. G. Parr, *Phys. Rev. B* **1988**, *37*, 785–789.
- [50] B. Miehlich, A. Savin, H. Stoll, H. Preuss, *Chem. Phys. Lett.* **1989**, *157*, 200–206.
- [51] T. Yanai, D. P. Tew, N. C. Handy, *Chem. Phys. Lett.* **2004**, *393*, 51–57.
- [52] K. Pierloot, B. Dumez, P.-O. Widmark, B. O. Roos, *Theor. Chim. Acta* **1995**, *90*, 87–114.
- [53] P.-O. Widmark, B. J. Persson, B. O. Roos, *Theor. Chim. Acta* **1991**, *79*, 419–432.
- [54] P.-O. Widmark, P.-Å. Malmqvist, B. O. Roos, *Theor. Chim. Acta* **1990**, *77*, 291–306.
- [55] G. Ghigo, B. O. Roos, P. Å. Malmqvist, *Chem. Phys. Lett.* **2004**, *396*, 142–149.
- [56] N. Forsberg, P. Å. Malmqvist, *Chem. Phys. Lett.* **1997**, *274*, 196–204.
- [57] D. Roca-Sanjuán, A. Francés-Monerris, I. F. Galván, P. Farahani, R. Lindh, Y. J. Liu, in *Photochemistry*, **2017**, pp. 16–60.
- [58] M. Navarrete-Miguel, J. Segarra-Martí, A. Francés-Monerris, A. Giussani, P. Farahani, B.-W. Ding, A. Monari, Y.-J. Liu, D. Roca-Sanjuán, in *Photochemistry*, **2018**, pp. 28–77.
- [59] L. Serrano-Andrés, D. Roca-Sanjuán, G. OlasoGonzález, in

- Photochemistry*, **2011**, pp. 10–36.
- [60] D. Roca-Sanjuán, I. Fdez. Galván, R. Lindh, Y. J. Liu, in *Photochemistry*, **2015**, pp. 11–42.
- [61] Y. J. Liu, D. Roca-Sanjuán, R. Lindh, in *Photochemistry*, **2012**, pp. 42–72.
- [62] P. Farahani, D. Roca-Sanjuán, F. Zapata, R. Lindh, *J. Chem. Theory Comput.* **2013**, *9*, 5404–5411.
- [63] L. De Vico, Y.-J. Liu, J. W. Krogh, R. Lindh, *J. Phys. Chem. A* **2007**, *111*, 8013–8019.
- [64] P. Farahani, M. Lundberg, R. Lindh, D. Roca-Sanjuán, *Phys. Chem. Chem. Phys.* **2015**, *17*, 18653–18664.
- [65] L. De Vico, M. Olivucci, R. Lindh, *J. Chem. Theory Comput.* **2005**, *1*, 1029–1037.
- [66] D. Roca-Sanjuán, G. Olaso-González, I. González-Ramírez, L. Serrano-Andrés, M. Merchán, *J. Am. Chem. Soc.* **2008**, *130*, 10768–10779.
- [67] A. Giussani, M. Merchán, J. P. Gobbo, A. C. Borin, *J. Chem. Theory Comput.* **2014**, *10*, 3915–3924.
- [68] P. Å. Malmqvist, B. O. Roos, B. Schimmelpfennig, *Chem. Phys. Lett.* **2002**, *357*, 230–240.
- [69] B. A. Heß, C. M. Marian, U. Wahlgren, O. Gropen, *Chem. Phys. Lett.* **1996**, *251*, 365–371.
- [70] S. F. Boys, F. Bernardi, *Mol. Phys.* **2002**, *100*, 65–73.
- [71] G. Olaso-González, D. Roca-Sanjuán, L. Serrano-Andrés, M. Merchán, *J. Chem. Phys.* **2006**, *125*, 231102.